Research Article | Vol. 10, No. 2 | 1 Feb 2019 | BIOMEDICAL OPTICS EXPRESS 1032
Biomedical Optics EXPRESS

Scanning optical coherence tomography probe for in vivo imaging and displacement measurements in the cochlea

NATHAN C. LIN,[1] ELIKA FALLAH,[2] C. ELLIOTT STRIMBU,[3] CHRISTINE P. HENDON,[1] AND ELIZABETH S. OLSON[2,3,*]

[1]*Department of Electrical Engineering, Columbia University, 500 W. 120th St., Mudd 1310, New York, NY 1002, USA*
[2]*Department of Biomedical Engineering, Columbia University, 1210 Amsterdam Ave, New York, NY 10027, USA*
[3]*Department of Otolaryngology, Head and Neck Surgery, Columbia University Medical Center, 180 Fort Washington Ave., NY 10032, USA*
**eao2004@columbia.edu*

Abstract: We developed a spectral domain optical coherence tomography (SDOCT) fiber optic probe for imaging and sub-nanometer displacement measurements inside the mammalian cochlea. The probe, 140 μm in diameter, can scan laterally up to 400 μm by means of a piezoelectric bender. Two different sampling rates are used, 10 kHz for high-resolution B-scan imaging, and 100 kHz for displacement measurements in order to span the auditory frequency range of gerbil (~50 kHz). Once the cochlear structures are recognized, the scanning range is gradually decreased and ultimately stopped with the probe pointing at the selected angle to measure the simultaneous displacements of multiple structures inside the organ of Corti (OC). The displacement measurement is based on spectral domain phase microscopy. The displacement noise level depends on the A-scan signal of the structure within the OC and we have attained levels as low as ~0.02 nm in in vivo measurements. The system's broadband infrared light source allows for an imaging depth of ~2.7 mm, and axial resolution of ~3 μm. In future development, the probe can be coupled with an electrode for time-locked voltage and displacement measurements in order to explore the electro-mechanical feedback loop that is key to cochlear processing. Here, we describe the fabrication of the laterally-scanning optical probe, and demonstrate its functionality with in vivo experiments.

1. Introduction

Spectral Domain Optical Coherence Tomography (SDOCT) is a low-coherence interferometric system developed mainly for imaging, and also capable of displacement measurements, using Spectral Domain Phase Microscopy (SDPM) [1]. SDOCT has a penetration depth of several millimeters, resulting from working in the infrared range, and the ability to simultaneously measure displacements at locations all along the axial-scan (A-scan). Its steep optical sectioning curve, based on its broadband light source, results in ~3 μm axial resolution [2]. This resolution is adequate for displacement measurements in the sensory tissue of the cochlea, whose different structures are separated by distances on the order of 10 μm. Following pioneering work over the past decade [3–5], the data generated by OCT systems is having a substantial impact on the understanding of cochlear processing. Several groups, including ours, have performed SDOCT-based displacement measurements using a Thorlabs system (*Telesto III*), which is designed for imaging and can be tailored by the user for phase-based displacement measurements [6,7]. The light source of the Telesto III is comprised of two coupled superluminescent diodes, with a central wavelength of ~1300 nm

#351849 https://doi.org/10.1364/BOE.10.001032
Journal © 2019 Received 15 Nov 2018; revised 15 Jan 2019; accepted 15 Jan 2019; published 1 Feb 2019

Biomedical Optics EXPRESS

and a bandwidth of ~135 nm. The system's axial resolution, Δz, is 3.5 μm in air and in saline-rich tissue like the cochlea, the index of refraction n ~1.3, and Δz is 2.7 μm.

To date, we have used the Telesto as a bulk-optics SDOCT system to measure displacements of the cochlea's sensory tissue through the transparent round window membrane (RWM), at the base of the cochlea [2,6]. Other auditory groups have measured through the bony shell in the apical region of the cochlea where the bone is relatively thin [3]. The access locations are limited because the cochlea is surrounded by bone, and damage will modify the measured displacements, in particular by reducing the active outer-hair-cell-based process termed cochlear amplification. Going from the apex to the base the frequency of sound processing increases, in humans from ~20 to ~20000 Hz and in gerbils from ~100 to 50000 Hz. The processing of sound is similar, but not identical, in the cochlear base and apex, and both regions are interesting scientifically. Our lab studies the basal cochlea, and the probe described here is being developed for measurements in that region, but could be used in the cochlear apex, as well as other applications. Here we demonstrate, through in vivo experiments, a fiber-optic-probe-based SDOCT system. In the current experiments we accessed the cochlea's sensory tissue through the RW, with intact RWM. The SMF/GRIN probe has a diameter of 140 μm, and can also be inserted via a hole (cochleostomy) drilled in the bone of ~200 x 500 μm (500 μm dimension to allow scanning). For many years our lab has used basal cochleostomies of ~200 μm diameter with fiber optic probes of ~150 μm without damaging the active cochlear process, in measurements in gerbil [8]. The presence of the persistent stapedial artery makes larger holes difficult in the gerbil base, but cochleostomies of ~400 – 500 μm have been made in the base and apex of chinchilla and guinea pig cochleae for imaging and motion measurements [9].

We had two motivations for developing the probe system. Firstly, it will allow us to access locations that the bulk-optics system cannot access. Secondly, we plan in the future to attach an electrode to the side of the probe, in order to make simultaneous displacement and outer hair cell (OHC)-produced voltage measurements. A similar pressure-voltage dual sensor, built around a fiber-optic probe, was developed previously by our lab [8]. With our planned electrode/SD-OCT probe, the measurements of voltage and motion will be coincident in both time and space, and will allow us to explore the electro-mechanical feedback loop that results in cochlear amplification.

SDOCT displacement measurements with a fiber optic probe have been performed previously. For example, optical coherence elastography determines tissue displacement produced by compressive loading [10–13], using probe-based SDOCT. Probe-based displacement measurements have not been done in the cochlea, although several groups have imaged the cochlea with fiber optic probes that scan by rotating around the long axis [14,15], and another group has developed a fiber optic probe for middle-ear imaging [16].

In this paper, we describe the development and initial use of an SDOCT probe with controllable lateral scanning up to 400 μm. This scanning range is suitable for identifying cochlear structures. Once the structures are identified, the scanning is stopped and the probe can be precisely pointed at a specific angle for subnanometer–scale displacement measurements of the structures along that angle's A-scan. Two in vivo experiments were done to validate the probe's usage.

2. Probe system

2.1 Probe design

The probe is composed of a micro-GRIN fiber ~140 μm in diameter, with g = 5.9 mm^{-1}, a length of 500 μm, fused to SMF-28 fiber. This basic component was ordered from *WT&T Inc, Pierrefonds, Quebec Canada*. A micrograph is shown in Fig. 1(A). A probe-measured A-scan of a water-immersed mirror is shown in Fig. 1(B). The beam profile was measured by the manufacturer with a BeamScan Optical profiler placed at the focal point (focal length = 250

Biomedical Optics EXPRESS

μm). The profiles are shown in Fig. 1(C) and Fig. 1(D), and have a spot size of 11 and 12 μm in the x and y-axes respectively. This spot size matches reasonably well with the theoretical ray tracing matrix analysis for GRIN lenses [17–19]. Based on ray tracing analysis, the probe's focal distance is increased by a factor of 1.3 when used in water instead of air, whereas the beam waist remains unchanged [17]. The probe is held in a glass capillary that is adhered to the end of a piezoelectric bender (Fig. 1(E)). The bender is a piezoelectric bimorph, 2.5 cm x 0.6 cm x 0.05 cm, adhered with epoxy to an aluminum rod. Similar benders are available from Thorlabs (e.g., part # PB4NB2W). The probe is held by a three-dimensional micro-manipulator (three-axis micro-manipulator, *World Precision Instruments*) that is attached to the optical table. For the in vivo experiments in gerbil, the probe imaged through the transparent RWM (Fig. 1(F)) following opening of the bulla.

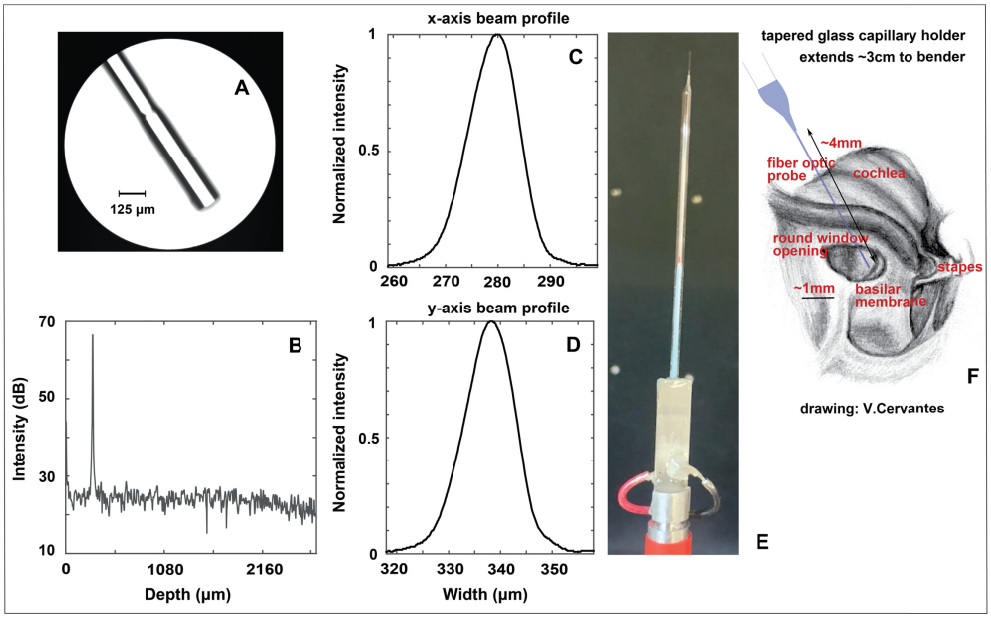

Fig. 1. A. Microscope image of the probe. B. The A-scan of a water-immersed mirror measured by the probe. The full width at half maximum is 12 μm. C, D. Measured beam profile in the x and y-axes. E. Photograph of the probe on the piezoelectric bender. F. Probe insertion schematic for the in vivo experiments.

The probe is used in a noncommon-path (nonCP) setup for imaging. This setup uses an external reference arm containing a polarization controller, collimator, iris diaphragm, and a retro-reflector (Fig. 2). This allows for fine-tuning of the reference beam intensity by controlling the iris diaphragm and the angle of the retro-reflector. Once the structures are recognized, the probe is centered at the desired angle (with a DC voltage controlling the piezoelectric bender) while scanning (with a sawtooth voltage waveform controlling the bender). The scanning range is gradually decreased and ultimately stopped to position the probe pointing at the cochlear sensory tissue. At this point, we switch the probe to the common-path (CP) setup (blue line). CP setup increases the amount of light to the sample, raising the signal-to-noise ratio (SNR) in the displacement measurement. The displacement measurement is then done at the sample rate of 97 kHz.

Biomedical Optics EXPRESS

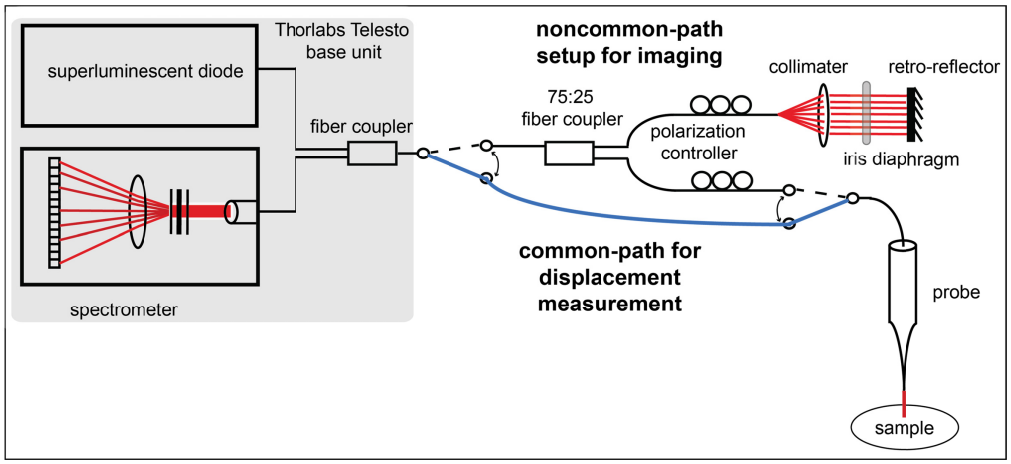

Fig. 2. Probe setup is nonCP for imaging, which uses an external reference arm containing a polarization controller, collimator, iris diaphragm, and a retro-reflector. Once the cochlear structures are recognized, the probe is centered at the desired angle (with the DC voltage controlling the piezoelectric bender that is holding the probe) while scanning (with the sawtooth voltage waveform controlling the bender). The scanning range is gradually decreased and ultimately stopped to position (with only the DC voltage) the probe at the cochlear sensory tissue. We then switched to the CP setup (shown in the blue line).

2.2. Scanning

To implement lateral scanning and angle positioning, the driving signal for the Telesto x-axis scanner is tapped from the Telesto base unit. By using the Telesto signal for scanning, the probe's scanned output can be viewed using the Telesto's real-time imaging software, *ThorImage*. The driving signal is modified and delivered to a piezoelectric-bender probe-holder for scanning [20]. The flow diagram of the modification circuitry is shown in Fig. 3. The tapped signal (Fig. 3(A)) is a ~1-second periodic sawtooth. The ~1 second period is obtained by operating *ThorImage* in the 2-D imaging mode, with the sampling rate (a parameter in the software) set to 10 kHz. When attached to the bender, the probe tip moves ~1 µm/volt. Problematically, the sawtooth waveform contains sharp transitions and a voltage spike at the end of each cycle. These are problematic because they contain many frequency components, including components around the bender's mechanical resonance frequency, ~270 Hz. A series of circuitry steps was used to adequately reduce the problematic frequency components, and to control the lateral scanning range and final probe angle. These steps are outlined below.

A summing amplifier is first used to increase the amplitude of the driving waveform by a factor of 10 (and invert it), and to add a DC voltage that shifts the spike out of the power supply range. (Alternatively, the spike can be eliminated with software configuration.) The modified (de-spiked) waveform (Fig. 3(B)) is then low-pass filtered and AC coupled, and sent to a potentiometer-controlled voltage divider to adjust the waveform's amplitude, which controls the lateral Field of View (FOV) of the bender. This waveform is combined with a variable DC voltage in a second summing amplifier to position the bender at a desired angle while scanning. The modified driving signal is ultimately sent to an x20 piezo driver (Piezo Systems, *EPA-008-1*) and then to the piezoelectric bender, giving a maximum lateral scanning FOV of 400 µm.

The DC voltage determines the angle at which the probe is centered, while the sawtooth voltage determines the lateral scanning range. The combination of the two (DC voltage and the sawtooth waveform controlling the piezoelectric bender) allows for the probe to be centered at the desired angle while scanning, followed by the decreasing scanning range. The probe is ultimately stopped for displacement measurements at the selected angle.

Biomedical Optics EXPRESS

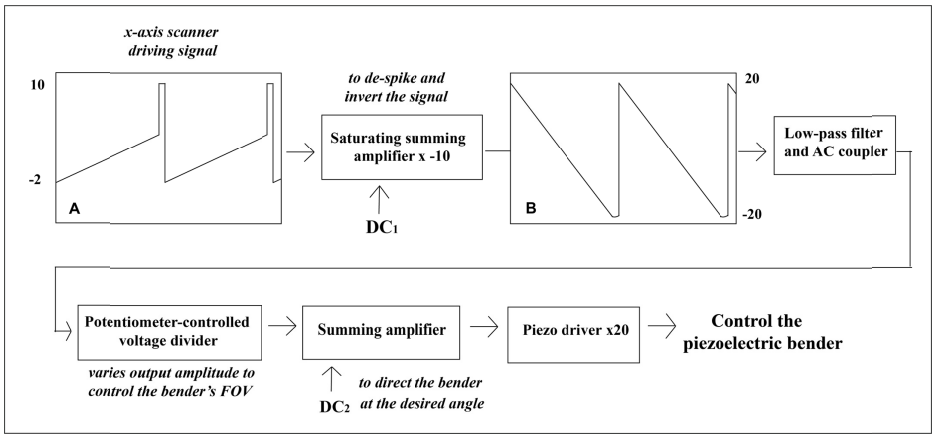

Fig. 3. Flow diagram for the modification steps for the signal that drives the bender. A. The original driving signal tapped from the Telesto x-axis scanner has a spike at the end of each period. B. By adding a DC voltage, the spikes are shifted out of the power supply range. Next, the de-spiked signal is low-pass filtered and AC coupled. Then a potentiometer-controlled voltage divider controls the amplitude of the driving signal to vary the scanning FOV. (See Visualization 1 for demonstration.) A DC voltage added to the AC signal with a summing amplifier is used to control the bender "set" angle. The piezo driver multiplies the drive signal by x20.

2.3. Displacement measurement

As we have described previously, the Telesto system is synchronized to the Tucker-Davis Technologies (TDT) data acquisition hardware, to acquire time-locked displacement and ear canal pressure data [21]. Synchronization is done by exporting and modifying the TTL pulse train from the TDT to trigger the Telesto base unit. The Telesto and the TDT are synchronized at a sampling rate of 97 kHz, so the maximum frequency component in a Fast Fourier Transform (FFT) of the recorded time waveforms is ~48 kHz. For the data presented here, the M-scan data acquisition time was 10 s, giving a 0.1 Hz bandwidth in the FFT. Stimulus frequencies fit evenly within the stimulus time so each is represented in a single FFT bin. For stimulus delivery and data acquisition software we used the TDT visual design studio, and the Thorlabs' C + + SpectralRadar SDK (software development kit), which contains functions to control the acquisition rate, output file formatting, and scan pattern of the Telesto, with the Microsoft Visual Studio as the Integrated Development Environment (IDE).

The displacement measurement process has been described [1,2] and we briefly review it here. The SDOCT's line-camera outputs raw data D(λ), in terms of wavelength. The relevant aspect of D(λ) is the λ-dependent interference pattern due to the interference of sample and reference beams. This signal is S(λ). The light source has its own inherent λ dependence, which is accounted for as a first step. This is done by subtracting the reference signal, R(λ) from D(λ).

The slight difference in the processing procedures for probe and bulk-optics (bench-top Telesto system) is described in the following. When using the bulk-optics SDOCT system, R(λ) is acquired by diverting the sample beam with a mirror so that only the reference beam illuminates the photodetectors. In a probe system, this straightforward way of finding R(λ) is not possible, and a different strategy is employed. The probe is immersed into a medium similar to that in which it will be used, but far from a reflector, and a data set is taken to represent R(λ). We averaged a full data set of A-scans to produce a clean R(λ).

Then the process follows the same steps as for the bulk-optics and the probe systems: S(λ) is found as D(λ) – R(λ). S(λ) is interpolated into S(k), in the k-domain, and then Fourier-transformed to the z-domain, to output the complex A-scan, S(z). The magnitude of the

Biomedical Optics EXPRESS

complex A-scan gives the depth profile of the sample structures (Fig. 4(B)) [22]. A series of A-scans (~10^6 for 10s of acquisition) is taken at a fixed lateral position in rapid temporal succession, called the M-scan, to acquire data for the displacement measurement. Displacement, $\delta(t)$, of the sample is found by evaluating the phase variations $\Theta(t)$ of the complex A-scan at the location of the peak in the A-scan magnitude. Unwrapping is performed to undo phase jumps > π at adjacent time points. $\delta(t) = \Theta(t)/(2nk_0)$, where $k_o = 2\pi/\lambda_o$, and λ_o is the center wavelength of the light source. The resulting waveform, $\delta(t)$, is then Fourier-transformed to the frequency domain in order to find the magnitude and phase of the sample.

Cochlear measurements were done in vivo on Mongolian gerbils (Meriones unguiculatus). The animal experiments were approved by the Columbia University Institutional Animal Care and Use Committee and a full description of the surgical preparation and anesthetic regimen and acoustic setup can be found in other papers from our lab [23].

The current paper is focused on the probe and the in vivo animal experiments were done to demonstrate its utility; new physiological findings are not a component of this paper. The measurements here were done in vivo in passive cochleae, following an independent set of measurements. In order to compare the results with those of the bulk optics system these data were collected with the probe imaging the OC through the round window (Fig. 4).

3. Results

3.1 In vivo cochlea imaging and displacement measurements

The round window, where the probe accessed the cochlea, is indicated with a dotted line in a cross-sectional sketch of the cochlea in Fig. 4(A). The lateral scanning was initially ranged at 400 μm and the acquired B-scan (top image of Fig. 4(B)) can be compared to the sketch in Fig. 4(A) to identify the RWM, basilar membrane, organ of Corti, and Reissner's membrane. The probe was positioned at the desired angle with DC voltage applied to the bender and scanned with the sawtooth voltage. The lateral scanning range was gradually decreased, and ultimately stopped to point the probe at the desired location (shown in Fig. 4(B) with the red-dotted line, and its corresponding A-scan). An M-scan was then acquired for displacement measurements, while stimulating the ear canal with a set of tones as described in the next section. The first structure at depth location 300 μm is the RWM, followed by the organ of Corti complex structures at depth locations between 400 and 500 μm. Reissner's membrane is at ~650 μm.

Biomedical Optics EXPRESS

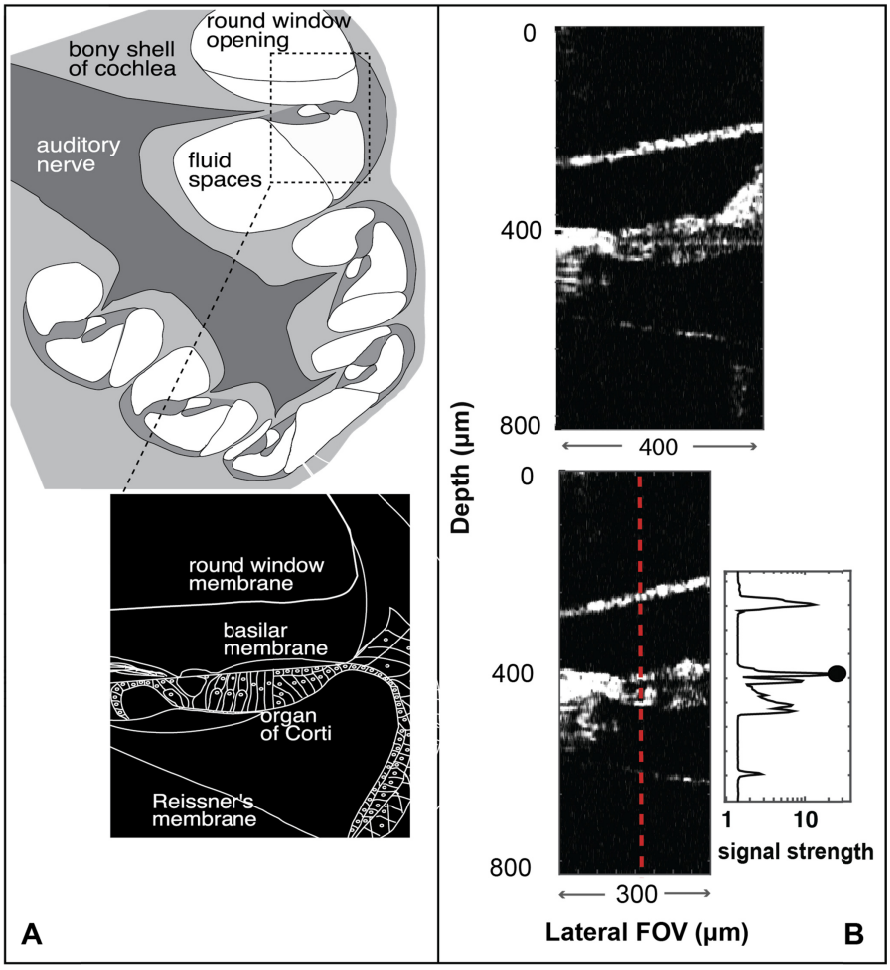

Fig. 4. A. Top shows a sketch of the cochlear cross-section. The probe accessed the cochlea's sensory tissue through the transparent round window. The boxed area is magnified in the lower sketch with the major cochlear structures labeled. B. The B-scan image with the scanning probe, showing the primary structures as in the magnified sketch. The lateral FOV of scanning was gradually decreased (one reduction step shown) and finally stopped for displacement measurements (A-scan location shown with the red dotted line).

A speaker tube coupled to a Fostex tweeter, and Sokolich ultrasonic microphone were positioned in the gerbil's ear canal, and a broadband 60-frequency stimulus tone was delivered, with each tone set at a level of ~60 dB SPL. The frequencies were unevenly spaced to reduce overlap of nonlinear components in the response [24]. The tones ranged from 4 to 37 kHz and spanned much the gerbil's hearing range [25,26]. The displacement of the BM, located at the 400 μm dotted position of Fig. 4, was determined.

The Fourier-transformed time-domain measurements are shown in the frequency domain (Fig. 5) with the stimulus in Fig. 5(A) and displacement response in Fig. 5(B). The displacement frequency spectrum has a noise floor ~0.02 nm. The displacement values with ~60 dB SPL stimuli range from ~0.05 to 1 nm, peaking at ~25 kHz. The peak is mild, as expected in a passive preparation. A passive peak at ~25 kHz in the basal region of the gerbil cochlea is consistent with previous measurements [27–29]. The magnitude of the measured displacement is also in line with previous measurements of BM motion in this region.

Biomedical Optics EXPRESS

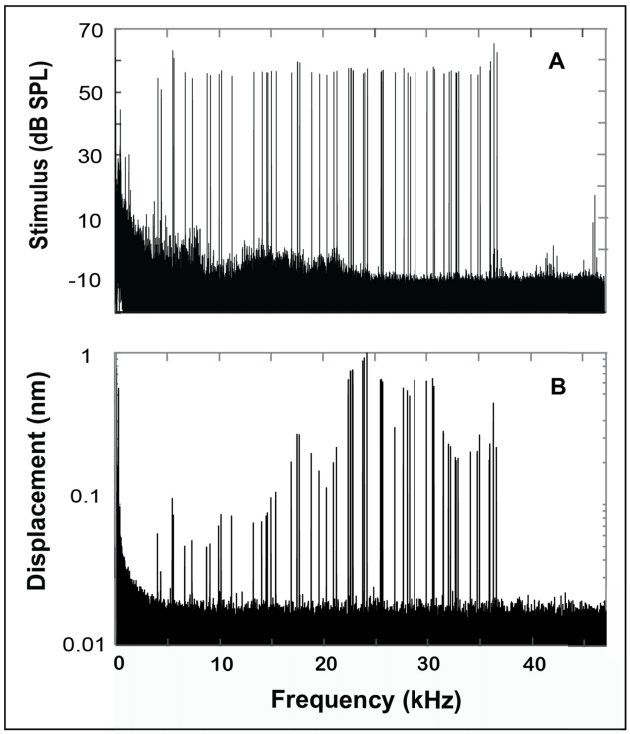

Fig. 5. A. The Fourier-transformed time domain stimulus at 60 dB SPL. B. The displacement frequency spectrum of the BM in the organ of Corti, with a noise floor ~0.02 nm.

3.2 In vivo cochlea displacement comparison between the bulk-optics and the probe SDOCT systems

To verify that the probe's displacement measurements are consistent with those obtained by the bulk-optics Telesto SDOCT system, we did a second in vivo experiment. We first obtained the B-scan of the cochlea with the bulk-optics system for structure recognition (shown in the middle image of Fig. 6(A)), followed by displacement measurements with the 60-frequency stimulus as in Fig. 5(A) delivered to the ear canal. Following the bulk-optics measurements, the probe was inserted at the same location and angle, and the displacement measurement repeated with the probe. The relative beam positions of the bulk-optics and probe measurements are plotted in the dotted lines in Fig. 6(A), based on their respective A-scans. We selected the most-reflective structure inside the OCC to measure the displacement responses, noted in the colored dots in the A-scans in the left and right diagrams of Fig. 6(A). The displacement frequency responses, plotted as gain re: stapes motion, and phase re: ear canal pressure are plotted in Fig. 6(B). The results are very similar and the slightly different amount of gain in the probe versus bulk-optics measurement can be explained by the 7 μm lateral position variation. The probe results are shown at 60 and 70 dB SPL and the responses scaled linearly. In a healthy cochlea the motion response of the OCC is nonlinear, but the linearity observed is expected since these measurements were performed in the base of the cochlea where cochlear activity is particularly fragile, at the end of a set of bulk-optics measurements. As noted in the introduction, new physiology is not a part of this paper and the linearity that was observed reassures that the probe operates linearly, as expected. As a final note, in previous work we have shown the Telesto bulk-optics displacement measurement agrees with that of a standard laser Doppler velocimeter [21]. These results give us confidence that the probe will be useful for in vivo physiological study of the cochlea.

Biomedical Optics EXPRESS

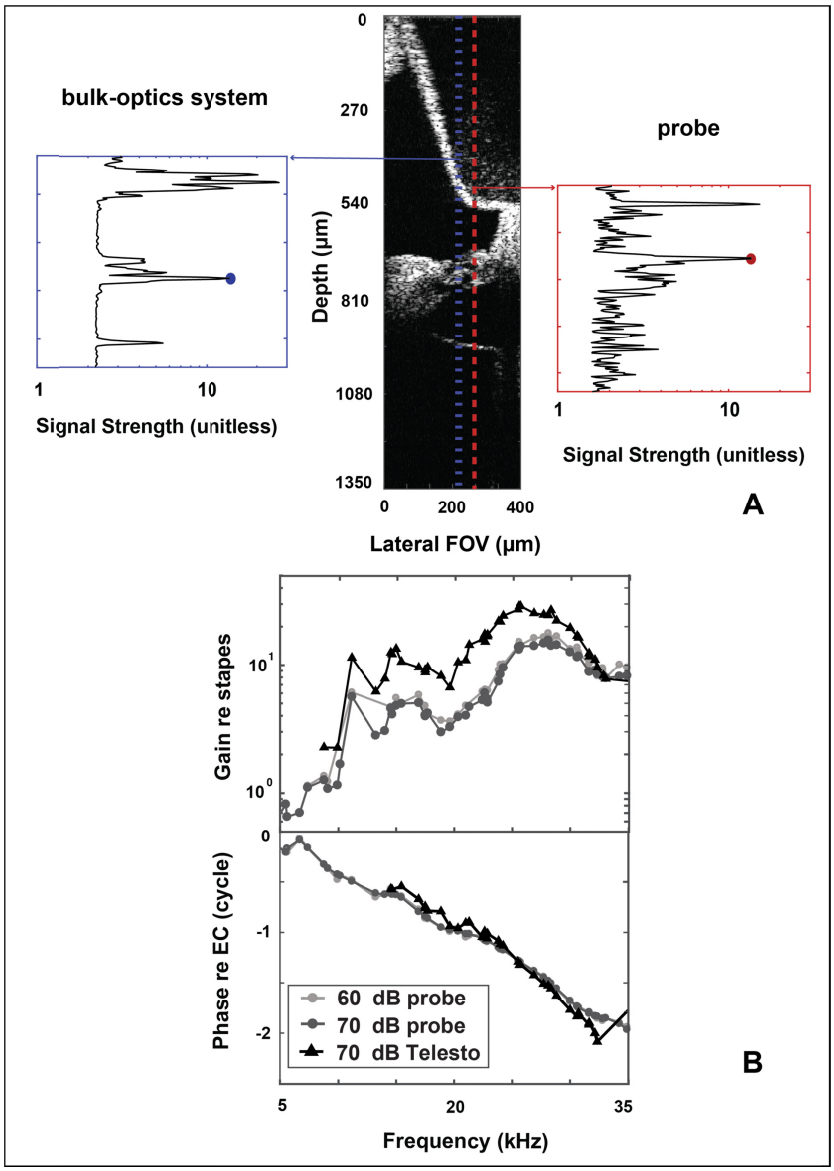

Fig. 6. A. The B-scan of the gerbil cochlea taken with the bulk optics SDOCT system. The RWM is at 540 μm, and the OC is at 600-800 μm. The bench-top and probe SDOCT were measured at the same location for displacement comparison. The bulk-optics' and probe's relative beam positions are plotted in the dotted lines, based on their measured A-scans shown on the sides of the B-scan image. The A-scans on the left and right are positioned vertically to coincide with the structures in the B-scan. B. The OC structures' tuning curves (magnitude referenced to the stapes) and the phases (referenced to the ear canal) are similar for both of the systems.

4. Discussion

In this study, we expanded upon present cochlear vibrometry approaches, LDV and bulk-optics SDOCT, to construct a laterally-scanning fiber-optic-probe-based imaging and displacement-measuring system. The narrow diameter of the probe allows access to the cochlear partition through the round window or through cochleostomies, providing flexibility in the access location. Once inside the cochlea, the probe can scan laterally for structural

Biomedical Optics EXPRESS

identification, and then be arrested to measure displacement along a selected A-scan. In addition, in the future an electrode can be coupled to the probe in order to simultaneously measure mechanical and electrical cochlear responses, to explore cochlear electromechanical processing [8].

Attaining a good SNR (a low displacement noise floor) for intracochlear measurements, especially deep inside the organ of Corti, is challenging because of the low reflectivity of the sensory tissue. For example, the outer hair cell reflectivity is only ~0.006% [30]. Our cochlear measurements in Fig. 5 showed a noise floor of ~0.02 nm, similar to those obtained by our and other groups' vibrometry systems [25,26,31]. With this noise floor, displacement can be measured at low SPL in the basal region of the gerbil's cochlea. The CP setup is used for displacement measurement to maximize the light to the sample, because with the nonCP setup, light is lost when traveling back and forth through a 75:25 fiber coupler. Additionally, by using the same optical path for both the sample and reference arms, systematic noise is reduced. On the other hand, the nonCP setup allows for adjustment of the reference beam level which is sometimes needed for real-time imaging.

As discussed in section 2.3, when using SDPM, displacement is determined from the phase variation of the complex A-scan peaks over time, and the minimum detectable phase difference $\sigma_{\Delta\Phi}$ in the complex A-scan sets the noise floor of the displacement measurements, δx. $\sigma_{\Delta\Phi}$ is directly related to the SNR of the A-scan's magnitude (SNR_A = the ratio of a reflector (peak) intensity to the background intensity, and the A-scan magnitude can be used to find an approximation for the displacement noise floor. The expression is: $\delta x = \frac{\lambda_0}{4n\pi}\sigma_{\Delta\phi} = \frac{\lambda_0}{4n\pi}\frac{2}{\pi}[\frac{1}{SNR_A}]^{\frac{1}{2}}$ [32,33]. The predicted δx for the bright structure in the organ of Corti in the experiment of Fig. 5 is 12 nm based on the SNR_A of the reflector's A-scan magnitude. Taking the frequency domain FFT lowers the noise floor because the noise is distributed among all the frequency bins (524288). This lowers (improves) the noise floor by a factor of $\frac{1}{\sqrt{number\_of\_frequency\_bins}}$, giving a theoretical δx of 0.0165 nm. This prediction is born out in the value of the experimental noise floor in Fig. 5(B).

5. Conclusion

We demonstrated a lateral scanning SDOCT probe, 140 μm in diameter, coupled to a Thorlabs Telesto SDOCT, for real-time laterally-scanned B-scans within the cochlea and displacement measurements with a noise floor of ~0.02 nm. Planned work includes coupling an electrode to the probe to explore the electro-mechanical feedback loop that results in cochlear amplification. In future work, the probe could be used to image and measure displacement in locations that can be accessed through a sub-mm-sized hole.

Funding

NIDCD (R01DC015362)

Disclosures

The authors declare that there are no conflicts of interest related to this article

References

1. M. A. Choma, A. K. Ellerbee, C. Yang, T. L. Creazzo, and J. A. Izatt, "Spectral-domain phase microscopy," Opt. Lett. **30**(10), 1162–1164 (2005).
2. N. C. Lin, C. P. Hendon, and E. S. Olson, "Signal Competition in optical coherence tomography and its relevance for cochlear vibrometry," J. Acoust. Soc. Am. **141**(1), 395–405 (2017).
3. H. Y. Lee, P. D. Raphael, J. Park, A. K. Ellerbee, B. E. Applegate, and J. S. Oghalai, "Noninvasive in vivo imaging reveals differences between tectorial membrane and basilar membrane traveling waves in the mouse cochlea," Proc. Natl. Acad. Sci. U.S.A. **112**(10), 3128–3133 (2015).

Biomedical Optics EXPRESS

4. R. K. Wang and A. L. Nuttall, "Phase-sensitive optical coherence tomography imaging of the tissue motion within the organ of Corti at a subnanometer scale: a preliminary study," J. Biomed. Opt. **15**(5), 056005 (2010).
5. S. S. Hong and D. M. Freeman, "Doppler optical coherence microscopy for studies of cochlear mechanics," J. Biomed. Opt. **11**(5), 054014 (2006).
6. E. Fallah, C. E. Strimbu, and E. S. Olson, "Outer hair cell and Basilar membrane responses to Zwuis tone complexes," Abstracts of the 41th Midwinter research meeting, Association for Research in Otolaryngology, PS 696 (2018).
7. N. Cooper and M. van der Heijden, "Spatial profiles of sound-evoked vibration in the gerbil cochlea," AIP Conference Proceedings **1965**, C. Bergevin, S. Puria, eds. (2018), p. 080001.
8. W. Dong and E. S. Olson, "Detection of cochlear amplification and its activation," Biophys. J. **105**(4), 1067–1078 (2013).
9. W. S. Rhode, "Basilar membrane mechanics in the 6-9 kHz region of sensitive chinchilla cochleae," J. Acoust. Soc. Am. **121**(5 Pt1), 2792–2804 (2007).
10. Y. Qiu, Y. Wang, Y. Xu, N. Chandra, J. Haorah, B. Hubbi, B. J. Pfister, and X. Liu, "Quantitative optical coherence elastography based on fiber-optic probe for in situ measurement of tissue mechanical properties," Biomed. Opt. Express **7**(2), 688–700 (2016).
11. L. Chin, A. Curatolo, B. F. Kennedy, B. J. Doyle, P. R. T. Munro, R. A. McLaughlin, and D. D. Sampson, "Analysis of image formation in optical coherence elastography using a multiphysics approach," Biomed. Opt. Express **5**(9), 2913–2930 (2014).
12. K. M. Kennedy, B. F. Kennedy, R. A. McLaughlin, and D. D. Sampson, "Needle optical coherence elastography for tissue boundary detection," Opt. Lett. **37**(12), 2310–2312 (2012).
13. B. F. Kennedy, R. A. McLaughlin, K. M. Kennedy, L. Chin, A. Curatolo, A. Tien, B. Latham, C. M. Saunders, and D. D. Sampson, "Optical coherence micro-elastography: mechanical-contrast imaging of tissue microstructure," Biomed. Opt. Express **5**(7), 2113–2124 (2014).
14. J. Lin, H. Staecker, and M. S. Jafri, "Optical Coherence Tomography Imaging of the Inner Ear: A Feasibility study with Implications for Cochlear Implantation," Ann. Otol. Rhinol. Laryngol. **117**(5), 341–346 (2008).
15. S. S. Gurbani, P. Wilkening, M. Zhao, B. Gonenc, G. W. Cheon, I. I. Iordachita, W. Chien, R. H. Taylor, J. K. Niparko, and J. U. Kang, "Robot-assisted three-dimensional registration for cochlear implant surgery using a common-path swept-source optical coherence tomography probe," J. Biomed. Opt. **19**(5), 057004 (2014).
16. M. E. Pawlowski, S. Shrestha, J. Park, B. E. Applegate, J. S. Oghalai, and T. S. Tkaczyk, "Miniature, minimally invasive, tunable endoscope for investigation of the middle ear," Biomed. Opt. Express **6**(6), 2246–2257 (2015).
17. W. A. Reed, M. F. Yan, and M. J. Schnitzer, "Gradient-index fiber-optic microprobes for minimally invasive in vivo low-coherence interferometry," Opt. Lett. **27**(20), 1794–1796 (2002).
18. W. L. Emkey and C. Jack, "Analysis and Evaluation of Graded-Index Fiber-Lenses," J. Lightwave Technol. **5**(9), 1156–1164 (1987).
19. Y. Mao, S. Chang, S. Sherif, and C. Flueraru, "Graded-index fiber lens proposed for ultrasmall probes used in biomedical imaging," Appl. Opt. **46**(23), 5887–5894 (2007).
20. D. P. Corey and A. J. Hudspeth, "Mechanical stimulation and micromanipulation with piezoelectric bimorph elements," J. Neurosci. Methods **3**(2), 183–202 (1980).
21. N. C. Lin, C. E. Strimbu, C. P. Hendon, and E. S. Olson, "Adapting a Commercial Spectral Domain Optical Coherence Tomography System for Time-locked Displacement and Physiological Measurements". AIP Conference Proceedings **1965**,. C. Bergevin, S. Puria, eds. (2018), p. 080004.
22. J. A. Izatt and M. A. Choma, *Theory of Optical Coherence Tomography. In: Optical Coherence Tomography: Technology and Applications* (Springer, 2015).
23. Y. Wang and E. S. Olson, "Cochlear perfusion with a viscous fluid," Hear. Res. **337**, 1–11 (2016).
24. M. van der Heijden and P. X. Joris, "Cochlear phase and amplitude retrieved from the auditory nerve at arbitrary frequencies," J. Neurosci. **23**(27), 9194–9198 (2003).
25. N. P. Cooper, A. Vavakou, and M. van der Heijden, "Vibration hotspots reveal longitudinal funneling of sound-evoked motion in the mammalian cochlea," Nat. Commun. **9**(1), 3054 (2018).
26. C. E. Strimbu, N. C. Lin, and E. S. Olson, "Optical coherence tomography reveals complex motion between the basilar membrane and organ of Corti in the gerbil cochlea," Abstracts of the 175th meeting of the Acoustic Society of America **143**(3):1898 (2018).
27. E. H. Overstreet 3rd, A. N. Temchin, and M. A. Ruggero, "Basilar membrane vibrations near the round window of the gerbil cochlea," J. Assoc. Res. Otolaryngol. **3**(3), 351–361 (2002).
28. E. S. Olson, "Intracochlear pressure measurements related to cochlear tuning," J. Acoust. Soc. Am. **110**(1), 349–367 (2001).
29. T. Ren and A. L. Nuttall, "Basilar membrane vibration in the basal turn of the sensitive gerbil cochlea," Hear. Res. **151**(1-2), 48–60 (2001).
30. S. M. Khanna, C. J. Koester, J.-F. Willemin, R. Daendliker, and H. Rosskothen, "Noninvasive optical system for the study of the function of inner ear in living animals," SPIE **2732**, 64–81 (1996).
31. W. He, D. Kemp, and T. Ren, "Timing of the reticular lamina and basilar membrane vibration in living gerbil cochleae," eLife **7**, 1–17 (2018).
32. B. Park, M. C. Pierce, B. Cense, S.-H. Yun, M. Mujat, G. Tearney, B. Bouma, and J. de Boer, "Real-time fiber-based multi-functional spectral-domain optical coherence tomography at 1.3 µm," Opt. Express **13**(11), 3931–3944 (2005).

Biomedical Optics EXPRESS

33. S. Yazdanfar, C. Yang, M. Sarunic, and J. Izatt, "Frequency estimation precision in Doppler optical coherence tomography using the Cramer-Rao lower bound," Opt. Express **13**(2), 410–416 (2005).